Progress In Electromagnetics Research M, Vol. 97, 77–86, 2020

Design Analysis of One-Dimensional Photonic Crystal Based Structure for Hemoglobin Concentration Measurement

Amit K. Goyal*

Abstract—In this manuscript, a porous one-dimensional Photonic Crystal (1D-PhC) based sensor is designed for bio-chemical sensing application (i.e., hemoglobin concentration). The alternate layers of silicon are considered for design optimization, where the porosity is introduced to obtain the desired index contrast value. The sensing capability of the proposed design is enhanced by modifying the dispersion property of the structure. For this, a defect middle layer is deliberately introduced. The number of layers, defect layer optical thickness, and porosity values are optimized to confine a defect mode of desired wavelength. Finally, the detailed analysis of proposed structure is carried out. This provides the average sensitivity of around 323 nm/RIU (0.05 nm/(g/L) along with considerably higher Figure-of-merit (FOM) of 517 RIU^{-1}.

1. INTRODUCTION

The biomarker detection is a major requirement for early detection of various bio-chemical analytes. This involves development of highly sensitive devices those possess the capability to detect the minute concentration of biomarkers. Optical sensors have emerged as prominent devices those are widely employed for bio-sensing applications. This is because of their inherent advantages such as immunity towards electromagnetic interference, fast response time and label-free detection [1, 2]. Numerous label-free optical biosensors are proposed in the literature, in which Surface Plasmon Resonance (SPR) and Interferometer based techniques are considered to be more prominent [3–7]. Additionally, integration of PhC technology can further improve the device performance [8, 9]. This is because of its light guiding and confinement abilities. This improves the light-matter interaction, hence very good sensitivity at very small scale. The mentioned properties are widely explored and a number of PhC devices are proposed for various sensing applications [10–17].

Haemoglobin (HB) is one of the most important constituents of blood, who can help in detecting various dieses like thyroid dysfunction, diabetes and anaemia [18, 19]. Human blood is made of fix proportion of HB and plasma, whose RI depends on concentration of HB. Thereby, utilizing the RI based sensing mechanism, the HB concentration can easily be measured. A number of devices comprising 1D-PhC are already proposed for RI based sensing and HB concentration measurement [20–23]. Authors in Ref. [20] designed a ternary 1D-PhC waveguide structure for haemoglobin concentration measurement (0 to 50 g/L) and reported a sensitivity of around 51.46 nm/RIU. Recently in 2020, Goyal et al. [21] proposed a Bloch-surface-wave (BSW) based 1D-PhC structure in which a defect layer as a cover is introduced for sensing purpose. The authors monitored the shift in coupling angle by infiltrating various concentration of haemoglobin at the top air-dielectric interface and reported the average sensitivity of around 69°/RIU. Similarly, Hao et al. [22] proposed a superconductor material assisted 1D-PhC RI sensor for HB concentration measurement. Authors, considered alternate layers of superconductor and semiconductor materials to design the structure. This gives an average sensitivity of around

Received 6 August 2020, Accepted 23 September 2020, Scheduled 7 October 2020
* Corresponding author: Amit Kumar Goyal (amitgoyal.ceeri@gmail.com).
The author is with the ECE Department, Jaypee Institute of Information Technology, Noida-62, Uttar Pradesh 201309, India.

6.85789 µm/RIU and 6.48073 µm/RIU at a temperature of 80 K and 134 K respectively. Authors in [23] proposed an acoustic sensor using 1D-PhC and reported a sensitivity of around 3.314 MHz for a HB concentration variation of about 0 to 14%. The SPR based sensor is also explored for HB concentration measurement. Sharma et al. [24] designed a SPR based sensor that possesses the capability to detect HB concentration and provides a 0.005° resonance angel shift for a 1 g/L HB concentration. Researcher have also explored two dimensional (2D) PhC and PhC-fiber based techniques to detect HB concentration [25, 26] but they are not widely used because of their complex design and fabrication processes. The 1D-PhC structures can easily be fabricated using spin coating, dip coating or deposition techniques. Additionally, electro-chemical etching can also be used to fabricate homo-junction 1D-PhC structure. The most of the discussed 1D-PhC designs are made using hetero-structure that providing scattering and reflection losses at the internal interfaces. These structures also possesses comparably higher Full-width-half-maximum (FWHM), which directly affects the resolution and Figure-of-merit (FOM) of the sensing device. However, designing homogeneous structure these losses can be minimized, which results in improved sensitivity along with superior FOM and resolution.

In this paper, a homogeneous 1D-PhC design is proposed for bio-chemical sensing (haemoglobin concentration) applications. The proposed structure is designed using 1D-PhC made of silicon material, where refractive index contrast is managed by introducing porosity within different layers. Additionally, a defect layer is deliberately introduced between two uniform structures. The inclusion of defect layer modify the dispersion characteristics and leads to confinement of defect mode. The structural analysis is carried out using transfer matrix method (TMM). The infiltration of varying HB concentration affects the effective RI of defect layer. This results in confinement of defect modes of different wavelengths. Therefore, estimating the variation in defect mode wavelength with respect to change in analyte properties (concentration or refractive index), the HB concentration can be measured. The proposed design provides an average FWHM, FOM and sensitivity of around 0.6 nm, 517 RIU^{-1} and 0.05 nm/(g/L) (or 323 nm/RIU) respectively. The achieved sensor performance parameters are comparably much higher than the reported results in the literature. Additionally, the designed sensor also possesses the capability towards developing integrated sensor platform.

2. STRUCTURE DESIGN PRINCIPLE

The proposed 1D-PhC structure is designed considering silicon (Si) as material using quarter-wave Bragg stack. The physical and optical thicknesses of the Si are optimized to obtain a higher reflection centred at a wavelength of λ_o. The schematic representation of a proposed binary multilayer PhC structure is shown in Fig. 1. The structure comprises alternate layers of 'B' and 'A', having low RI (n_L) and high RI (n_H) respectively. The structural symmetry is modified by deliberately introducing a defect layer 'D'. The structure exhibits its periodicity (having Λ as the period) in the 'z' direction. The proposed design is homogeneous towards 'x' axis. Thus, refractive index profile can be represented by

$$n\left(z\right) = \begin{cases} n_L, & 0 < z < d_l \\ n_H, & d_l < z < d_l + d_h \end{cases} \qquad \text{with } n(z+\Lambda) = n(z) \tag{1}$$

where the z axis is normal to the interface of multilayer structure, and d_l & d_h are the thicknesses of two layers 'B' and 'A'. The capping of microfluidic channel is carried out to ease the analyte infiltration.

The TE polarised wave of central wavelength λ_o is incident on the structure from substrate side. Depending on the RI contrast and optical thicknesses, the structure will reflect some part of the incident wave at every interface. Thus, the optical thickness and RI contrast are optimized to obtain overall high reflection. Furthermore, defect layer ('D') properties are also modified to confine a defect mode within layer 'D'. Initially, the 1D-PhC structure possesses the form of substrate$|(\text{BA})^N|\text{D}|(\text{BA})^N|$air, where 'A', 'B' and 'D' are different layers as discussed previously, and 'N' corresponds to the number of stacks. Additionally, θ_H, θ_L, and θ_d are angle of reflection from layers 'A', 'B' and 'D' respectively and θ_a is the incident angle. The phase thicknesses within dielectric layers 'A' and 'B' can be calculated by Equation (2).

$$\delta_i = 2\pi \frac{f}{f_o} L_i \cos(\theta_i) \tag{2}$$

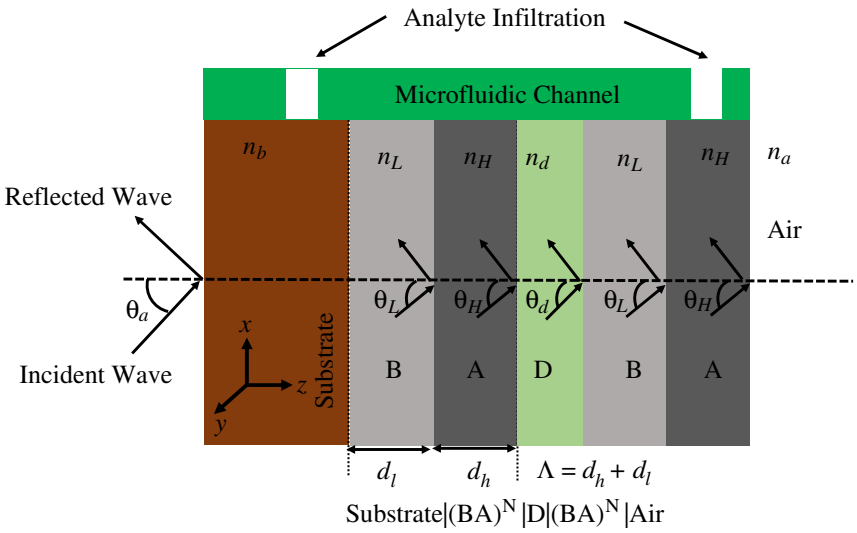

Figure 1. Schematic diagram of 1D-PhC structure. The structure possess 'A' and 'B' two alternate layer with 'D' as defect layer.

where L_i is the optical thickness of ith layers, normalized with central wavelength λ_o. Thus, infiltrating the analytes of different refractive index will impact the optical thickness of the ith layer. This changes the phase thickness hence shift in the confined defect mode wavelength. The structural analysis is carried out using TMM method in which amplitude components of forward (A_n) and backward (B_n) propagating plane waves are calculated using matrix method. The electric field amplitude in each layer (i.e., layer n) is obtained by solving Maxwell equations and are given by [27]

$$E(z,x) = A_n e^{ik_n z} + B_n e^{-ik_n z} \tag{3}$$

Equation (3) is solved for every interface, and corresponding field amplitudes are calculated. For example by applying the boundary conditions at first interface (layers 1 and 2), the solution of Equation (3) is represented by Equations (4) and (5)

$$\begin{pmatrix} A_1 \\ B_1 \end{pmatrix} = M_{12} \begin{pmatrix} A_2 \\ B_2 \end{pmatrix} \tag{4}$$

with

$$M_{12} = \begin{bmatrix} \frac{1}{2}\left(1+\frac{k_1}{k_2}\right)e^{ik_1 d_l} & \frac{1}{2}\left(1-\frac{k_1}{k_2}\right)e^{-ik_1 d_l} \\ \frac{1}{2}\left(1-\frac{k_1}{k_2}\right)e^{ik_1 d_l} & \frac{1}{2}\left(1+\frac{k_1}{k_2}\right)e^{-ik_1 d_l} \end{bmatrix} \tag{5}$$

Therefore, for finite size multilayer structure having n number of dielectric layers, Equation (4) can be generalized as

$$\begin{pmatrix} A_{n-1} \\ B_{n-1} \end{pmatrix} = M_n \begin{pmatrix} A_n \\ B_n \end{pmatrix} = \begin{pmatrix} M_1 & M_3 \\ M_2 & M_4 \end{pmatrix} \begin{pmatrix} A_n \\ B_n \end{pmatrix} \tag{6}$$

3. SIMULATION RESULTS AND DISCUSSION

The proposed structure is designed by sandwiching a defect layer 'D' between two uniform 1D-PhC structures. Initially, BK7 glass having refractive index 1.52 is considered as substrate to optimize the proposed 1D-PhC structure, $substrate|(BA)^N|D|(BA)^N|air$. The bulk Silicon (Si) is considered as a high (layer 'A') RI material whereas porous Silicon (P-si) having 50% porosity is considered as low (layer 'B') RI material. This gives the RI of around 3.45 and 2.34 for Si and P-Si respectively [28, 29]. The structure is designed to provide the maximum reflectance around a central wavelength of 1550 nm.

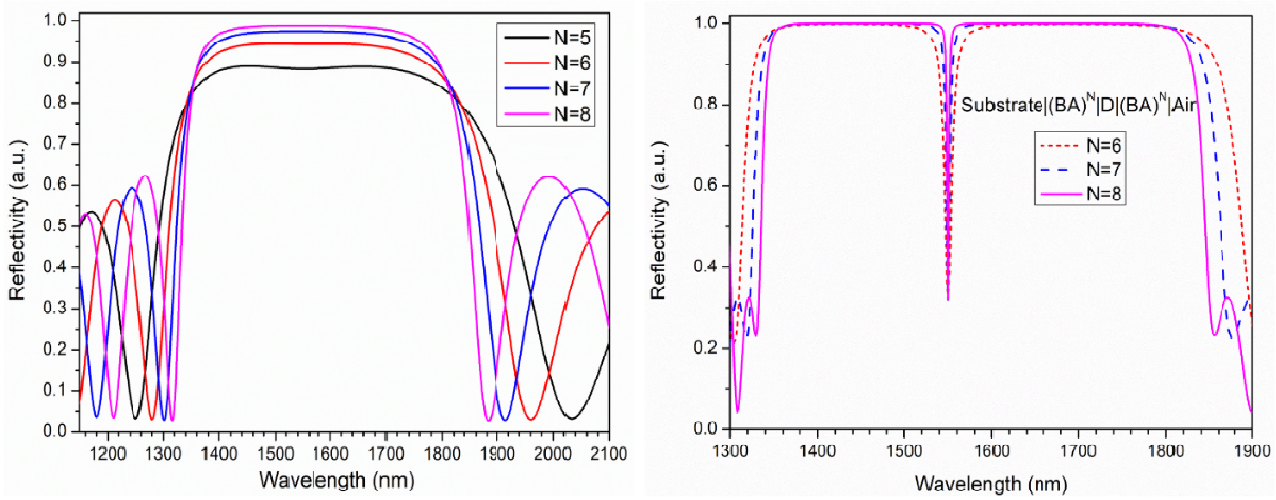

Figure 2. Effect of increasing number of layers on reflection spectrum for (a) substrate|(BA)|^N|Air and, (b) substrate|(BA)^N|D|(BA)^N|Air structure. The structure is designed at 50% porosity having $d_h = 112$ nm and $d_L = 166$ nm for central wavelength of 1550 nm.

Since the design is optimized to work at 1550 nm central wavelength thus, the imaginary RI or Si is neglected in the analysis. This also alleviates analytes induced scattering loss. Additionally, the pore size is also considered to be much smaller than the central wavelength [30].

The layers are organised in quarter-wave Bragg stack pattern. This provides the thicknesses of layers 'A' and 'B' of around 112 nm and 166 nm respectively. The numbers of layer in structure are optimized to obtain the overall high reflectivity at the central wavelength of 1550 nm as shown in Fig. 2(a). This clearly indicates that for $N = 6$ onward the reflectivity is more than 90%. Thus, six multilayer stacks are considered as initial optimized parameters in this case. The inclusion of defect layer 'D' results in a sharp dip in the reflection spectrum. Initially, the defect layer 'D' is considered to be equivalent to layer 'B' having same porosity, RI and thickness values. Fig. 2(b) shows the reflection spectrum of proposed structure having a defect layer, where a sharp dip is due to the incorporation of the defect layer. The FWHM of the dip depends of number of stacks. The structure substrate|(BA)^N|D|(BA)^N|Air confine the defect mode at 1550 nm having 70% dip intensity. The calculated FWHM values of the defect modes are around 12 nm, 6 nm and 2.5 nm for the corresponding number of stacks of $N = 6$, 7 and 8 respectively. Additionally, the confined defect mode wavelength can also by tuned to desired value by changing the defect layer optical thickness (physical thickness or refractive index value). Fig. 3 represents the effect of changing layer 'D' physical thickness (d_D) on confined defect mode wavelength for various porosity values of 50%, 60%, and 70%, respectively.

It is noteworthy to mention that for $d_D = d_L$, the structural parameters are optimized to confine the central wavelength of 1550 nm at every porosity. This results in the thicknesses of layer 'B' of around 166 nm, 184 nm, and 207 nm (having $d_h = 112$ nm) for the corresponding porosity of around 50%, 60% and 70% respectively. Therefore, for the defect mode thickness of $d_D = d_L$, the designed structure confines defect mode at the same central wavelength 1550 nm (central wavelength) for all porosities. However, increasing defect layer thickness to $1.2d_L$, the proposed structure confine defect mode at 1600 nm, 1610 nm and 1619 nm for the corresponding porosities of 50%, 60% and 70% respectively. Changing d_D from its original value (d_L) to $1.6d_L$ changes the defect mode wavelength of around 9%, 11% & 13% for the porosity of 50%, 60% and 70% respectively.

Figure 4 represents the sensing capability of the proposed structure for different porosity values of 50%, 60% and 70% respectively. The defect layer in infiltrated with various analytes of changing RI of 1.1, 1.2, 1.3 and 1.4 and this provides the wavelength shift in confined defect mode. Fig. 4(a) shows the sensing capability of proposed structure at 50% porosity and exhibits an average sensitivity of around

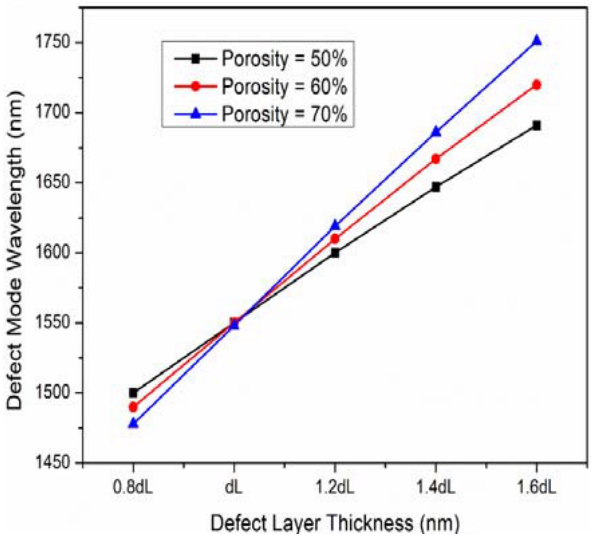

Figure 3. The effect of changing defect layer 'D' (d_D) thickness on defect mode wavelength for different porosity values.

133 nm/RIU. Similarly, Fig. 4(b) and Fig. 4(c) show the sensing capability of proposed structure for the porosity of 60% & 70% and exhibits an average sensitivity of around 186 nm/RIU and 261 nm/RIU respectively. Finally, Fig. 4(d) provides a detailed comparisons of above mention results. It is clear from Fig. 4(d) that increasing the porosity provides a larger shift in confined defect mode wavelength hence better sensitivity. Increasing the porosity can further improves the sensitivity but it is not considered as it makes the structure fragile. Therefore, in the rest of the paper, porous 1D-PhC cavity structure having 70% porosity and seven bilayers is considered for haemoglobin concentration analysis. The mentioned results are summarized in Table 1.

Table 1. Sensitivity comparison at three different porosity values.

Porosity	n_h	n_L	d_h (nm)	d_L (nm)	Defect mode Wavelength for air Analyte	Average Sensitivity (nm/RIU)
50%	3.45	2.34	112	166	1550 nm	133
60%	3.45	2.11	112	184	1550 nm	186
70%	3.45	1.87	112	207	1550 nm	261

3.1. Bio-Chemical (HB) Sensing Analysis

The refractive index (RI) of haemoglobin is measured by many groups, and their findings are reported [31, 32]. Barer et al. provided the concentration dependent RI of HB by considering oxygenated HBas shown in Equation (7) [33],

$$n_{hb} = \alpha_0 + \alpha C \tag{7}$$

$$\alpha_0 = 1.3245 + \frac{8.4052 \times 10^3}{\lambda^2} - \frac{3.9572 \times 10^8}{\lambda^4} - \frac{2.3617 \times 10^{13}}{\lambda^6} \tag{8}$$

C is the HB concentration (g/L), n_{hb} the RI of HB, α_0 the RI of solvent & given in Equation (8), λ the central incident wavelength (measured in nm), and $\alpha = 0.193$ mL/g the specific refraction increment [34, 35]. The haemoglobin RI increases along with its concentration. That further affects the effective RI of defect layer, hence change in confined defect mode wavelength. This

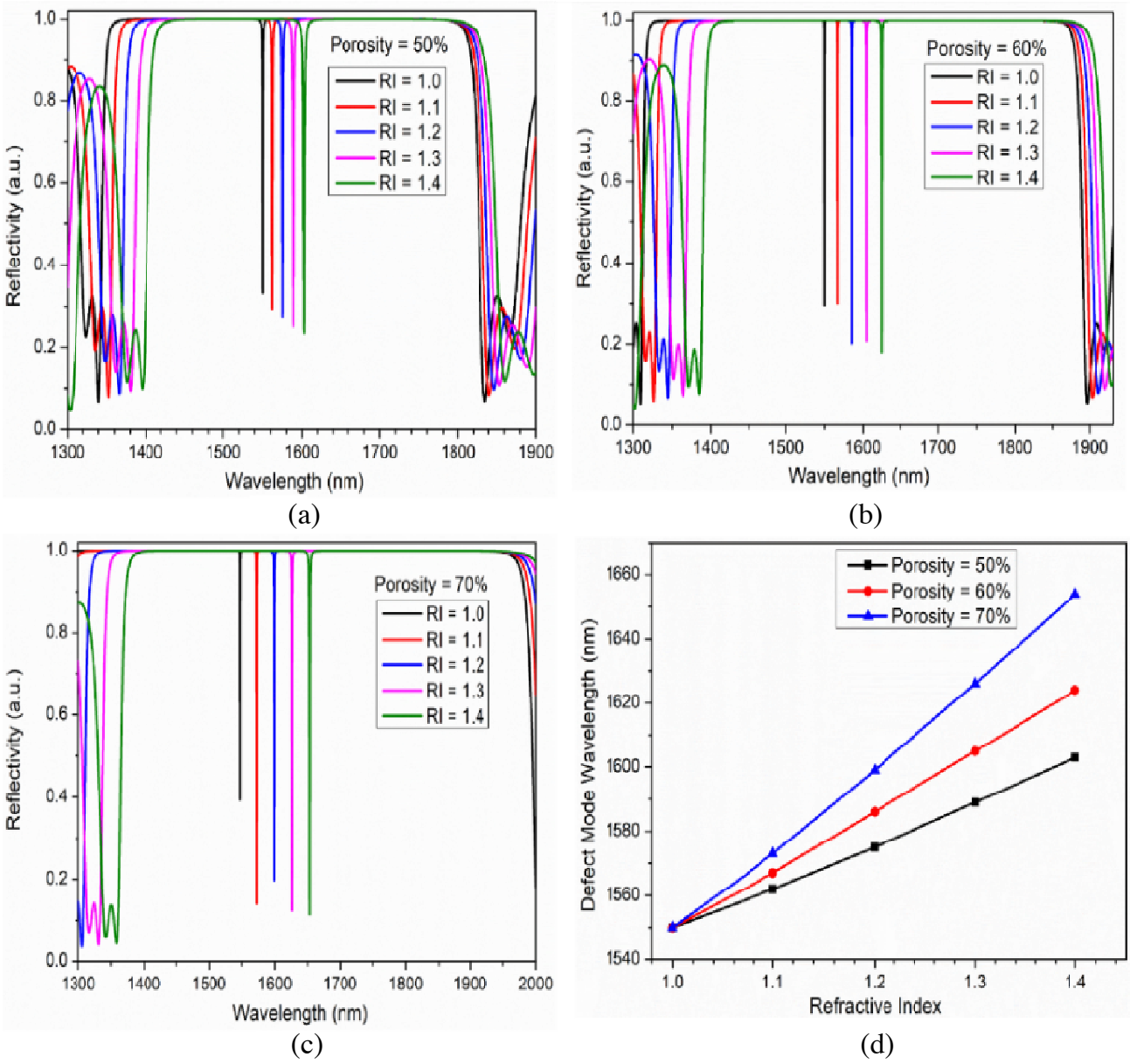

Figure 4. Sensing proficiency of proposed 1D-PhC at different porosities of (a) 50%, (b) 60%, (c) 70% and (d) combined comparison at all porosities. The structure is designed in substrate$|(\mathrm{BA})^N|\mathrm{D}|(\mathrm{BA})^N|$Air configuration.

defect mode wavelength is monitored to measure the concentration of haemoglobin. Considering Equations (7) and (8), the sensing capability of proposed structure is investigated to find the haemoglobin concentration. Fig. 5 represents the HB concentration dependent variation on confined defect mode wavelength.

The haemoglobin concentration is varied from 0 g/L to 200 g/L with the step of 40 g/L. The structure confines the defect modes having different wavelengths of 1634 nm, 1636 nm, 1638 nm, 1640 nm, 1642 nm and 1644 nm for the corresponding haemoglobin concentration of 0 g/L, 40 g/L, 80 g/L, 120 g/L, 160 g/L, and 200 g/L respectively. It is clear that at every increase in concentration, the defect mode wavelength is red shifted, whereas the FWHM is almost constant to a value of 0.6 nm. The performance parameters of the proposed design, i.e., sensitivity (S), FWHM, and Figure-of-merit (FOM) are also

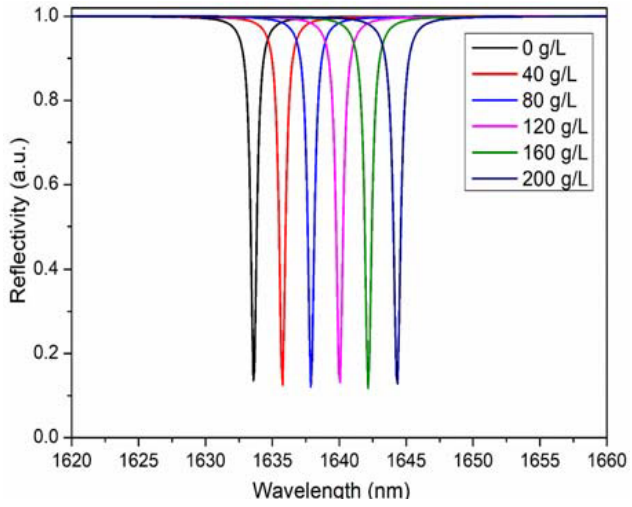

Figure 5. The effect of varying HB concentration on the defect mode wavelength.

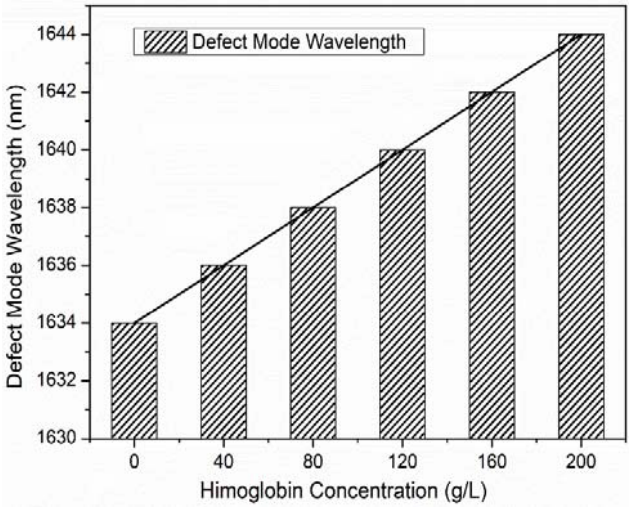

Figure 6. Effect of increasing HB concentration on defect mode wavelength.

analysed and shown in Equation (9) [36–38],

$$S = \frac{\Delta\lambda}{\Delta C} = \frac{\Delta\lambda}{\Delta n}$$
$$\text{FOM} = \frac{S}{\Delta\lambda_{1/2}} \tag{9}$$

where $\Delta\lambda$ and ΔC are the change in HB concentration and change in defect mode wavelength, and $\Delta\lambda_{1/2}$ is the FWHM. All these parameters are analysed and given in Table 2.

Table 2. Calculated performance parameters for the proposed sensor structure.

C	**ΔC**	**Δn**	$\boldsymbol{\lambda_d}$	$\boldsymbol{\Delta\lambda_d}$	$\boldsymbol{\Delta\lambda_{1/2}}$	**S**		**FOM**
(g/L)			**(nm)**			$\boldsymbol{(\Delta\lambda/\Delta n)}$	$\boldsymbol{(\Delta\lambda/\Delta C)}$	$\boldsymbol{(\text{RIU})^{-1}}$
0	-	-	1634	-	0.6	-	-	-
40	40	0.004	1636	2	0.6	500	0.05	833
80	80	0.012	1638	4	0.65	333	0.05	512
120	120	0.022	1640	6	0.65	272	0.05	418
160	160	0.031	1642	8	0.65	258	0.05	396
200	200	0.039	1644	10	0.6	256	0.05	426

It is evident from Table 2 that the defect mode wavelength changes from 1634 nm ($C_{\text{HB}} = 0$ g/L) to 1644 nm ($C_{\text{HB}} = 200$ g/L) for the structural porosity of 70%, having six number of bilayers. Fig. 6 represents the effect of increasing HB concentration of defect mode wavelength. The graph shows the almost linear variation, thus slope of the curve provides the average sensitivity ($S = \Delta\lambda/\Delta C$), which terms to be around 0.05 nm/(g/L) or 323 nm/RIU ($S = \Delta\lambda/\Delta n$). Similarly, the FWHM of the proposed design comes around 0.6 nm, which is comparably better than recent reported results [22, 23, 39]. This gives an overall high FOM of around 517 RIU^{-1}.

Equation (10) represents the linear fitting of Fig. 6, which represents the HB concentration dependent defect mode wavelength. Thus, Equation (10) can be used to determine the HB concentration (C).

$$\text{Defect Mode Wavelength } (\lambda_d) = 0.05C + 1634 \tag{10}$$

Additionally, the RI of blood can also be calculated by considering appropriate composition of haemoglobin (RBC) and plasma. The same is represented by Equation (11).

$$n_{\text{blood}} = n_{hb} \times f_{hb} + n_0 \times f_0 \tag{11}$$

where f_{hb} and f_0 are the volume fraction of haemoglobin and solvent respectively. Thereby, considering appropriate filling factors f_{hb} and f_0, its concentration can also be estimated directly from the blood sample. Table 3 represents the comparison of obtained results of designed 1D-PhC cavity structure with recently reported results.

Table 3. The comparison of proposed design with recent reported results.

Sensitivity	FWHM (nm)	FOM $(\text{RIU})^{-1}$	Year	Reference
69°/RIU	0.00508	-	2020	21
51.46 nm/RIU	-	-	2019	20
0.005°/g/L	-	-	2019	24
195 nm/RIU	-	-	2020	40
333 nm/RIU	-	16.66	2020	41
0.05 nm/(g/L) and 323 nm/RIU	0.6	517	Proposed	Proposed

4. CONCLUSION

A porous silicon based 1D-PhC cavity structure is designed for bio-chemical (haemoglobin concentration) sensing applications. The porosity is introduced to obtain the required index contrast value. The analysis depicts that the inclusion of a defect layer within two symmetrical 1D-PhC structures can confine a defect mode. Additionally, the defect mode wavelength can also be tuned by varying the porosity of the structure. The detailed performance analysis of the optimized structure is carried out. This gives an FWHM of around 0.6 nm with considerably improved sensitivity of around 0.05 nm/(g/L) or 323 nm/RIU. The linear dependency of HB concentration to defect mode wavelength facilitates the proposed 1D-PhC cavity structure to detect the HB concentration.

ACKNOWLEDGMENT

Author is thankful to all members of ECE department for their help and cooperation.

REFERENCES

1. Seitz, W. R., "Chemical sensors based on fiber optics," *Anal. Chem.*, Vol. 56, 16A, 1984.
2. Choi, C. J., et al., "Comparison of label-free biosensing in microplate, microfluidic, and spot-based affinity capture assays," *Analytical Biochemistry*, Vol. 405, No. 1, 1–10, 2010.
3. Ciminelli, C., et al., "Label free optical resonant sensors for biochemical applications," *Prog. Quant. Electron.*, Vol. 37, 51–107, 2013.
4. Homola, J., et al., "Surface plasmon resonance sensors: Review," *Sensors Actuators B*, Vol. 54, 3–15, 1999.
5. Karlsson, R. and R. Stahleberg, "Surface plasmon resonance detection and multispot sensing for direct monitoring of interactions involving low-molecular-weight analytes and for determination of low affinities," *Analytical Biochemistry*, Vol. 228, No. 2, 274–280, 1995.
6. Saleh, E. A. and M. C. Teich, *Fundamentals of Photonics*, Wiley-Interscience, Hoboken, New Jersey, 2007.
7. Bornhop, J., "Micro volume index of refraction determinations by interferometric backscatter," *Applied Optics*, Vol. 34, No. 18, 3234–3239, 1995.

8. Yablonovitch, E., "Inhibited spontaneous emission in solid-state physics and electronics," *Phys. Rev. Lett.*, Vol. 58, No. 20, 2059–2062, 1987.
9. Joannopoulos, J. D., et al., *Photonic Crystals: Molding the Flow of Light*, Princeton University Press, New Jersey, 2008.
10. Goyal, A. K. and S. Pal, "Design and simulation of high sensitive gas sensor using a ring-shaped photonic crystal waveguide," *Phys. Scr.*, Vol. 90, 025503, 2015.
11. Abd El-Aziz, O. A., et al., "One-dimensional defective photonic crystals for the sensing and detection of protein," *Appl. Opt.*, Vol. 58, 8309–8315, 2019.
12. Goyal, A. K. and S. Pal, "Design and simulation of high sensitive photonic crystal waveguide sensor," *Optik*, Vol. 126, No. 2, 240–243, 2015.
13. Goyal, A. K., et al., "Realization of large-scale photonic crystal cavity-based devices," *J. Micro./Nanolith. MEMS MOEMS*, Vol. 15, No. 3, 31608, 2016.
14. Chan, L. L., et al., "A method for identifying small-molecule aggregators using photonic crystal biosensor microplates," *Journal of the Association for Laboratory Automation*, Vol. 14, No. 6, 348–359, 2009.
15. Goyal, A. K., et al., "Performance optimization of photonic crystal resonator," *Opt. Quantum Electron.*, Vol. 48, 431, 2016.
16. Heeres, J. T., et al., "Identifying modulators of protein-protein interactions using photonic crystal biosensors," *Journal of the American Chemical Society*, Vol. 131, No. 51, 18202, 2009.
17. Goyal, A. K., et al., "Design and analysis of photonic crystal micro-cavity based optical sensor platform," *AIP Conference Proceedings*, Vol. 1724, 020005, 2016,
18. Beutler, E., et al., "The definition of anemia: What is the lower limit of normal of the blood hemoglobin concentration," *Blood*, Vol. 107, 1747–1750, 2006.
19. Ansarihadipour, H., et al., "Structural and spectroscopic changes of human hemoglobin during iron-mediated oxidative stress," *J. Arak. Univ. Med. Sci.*, Vol. 14, No. 6, 10–18, 2012.
20. El-Khozondar, H. J., et al., "Design of one dimensional refractive index sensor using ternary photonic crystal waveguide for plasma blood samples applications," *Physica E: Low-dimensional Systems and Nanostructures*, Vol. 111, 29–36, 2019.
21. Goyal, A. K., et al., "Design analysis of Bloch surface wave based sensor for haemoglobin concentration measurement," *Applied Nanoscience*, 2020, doi: 10.1007/s13204-020-01437-4.
22. Hao, J., et al., "Research on low-temperature blood tissues detection biosensor based on one-dimensional superconducting photonic crystal," *Communications in Nonlinear Science and Numerical Simulation*, Vol. 89, 105229, 2020.
23. Khateib, F., et al., "Ultra-sensitive acoustic biosensor based on a 1D phononic crystal," *Phys. Scr.*, Vol. 95, 075704, 2020.
24. Sharma, A. K., "Plasmonic biosensor for detection of hemoglobin concentra-tion in human blood: Design considerations," *J. Appl. Phys.*, Vol. 114, 044701, 2013.
25. Lidiya, A. E., et al., "Detecting hemoglobin content blood glucose using surface plasmon resonance in D-shaped photonic crystal fiber," *Opt. Fiber Technol.*, Vol. 50, 132–138, 2019.
26. Swain, K. P. and G. Palai, "Estimation of human-hemoglobin using honeycomb structure: An application of photonic crystal," *Optik*, Vol. 127, 3333–3336, 2016.
27. Pochi, Y., "Electromagnetic propagation in periodic stratified media. I. General theory," *J. Opt. Soc. Am.*, Vol. 67, No. 4, 423–438, 1977.
28. Ghosh, G., *Handbook of Thermo-optic Coefficients of Optical Materials with Applications*, Academic Press, 1998.
29. Goyal, A. K., et al., "Porous photonic crystal structure for sensing applications," *J. Nanophoton.*, Vol. 12, No. 4, 040501, 2018.
30. Khaleque, A., et al., "Absorption enhancement in graphene photonic crystal structures," *Applied Optics*, Vol. 55, 2936–2942, 2016.
31. Friebel, M., et al., "Determination of the complex refractive index of highly concentrated hemoglobin solutions using transmittance and reflectance measurements," *Journal of Biomedical*

Optics, Vol. 10, 064019–5, 2005.

32. Friebel, M., et al., "Model function to calculate the refractive index of native hemoglobin in the wavelength range of 250–1100 nm dependent on concentration," *Appl. Opt.*, Vol. 45, 2838–2842, 2006.
33. Barer, R., et al., "Refractometry and interferometry of living cells," *J. Opt. Soc. Am.*, Vol. 47, No. 6, 545–556, 1957.
34. Barer, R., et al., "Interference microscopy and mass determination," *Nature*, Vol. 169, 366, 1952.
35. Barer, R., et al., "Refractometry of living cells: Part I. Basic principles," *Quarterly Journal of Microscopical Science*, Vol. s3-95, 399–423, 1954.
36. White, I. M., et al., "On the performance quantification of resonant refractive index sensors," *Opt. Express*, Vol. 16, 1020–1028, 2008.
37. Goyal, A. K., et al., "Design and analysis of omnidirectional solar spectrum reflector using one-dimensional photonic crystal," *J. of Nanophotonics*, Vol. 14, No. 2, 026005, 2020, doi: 10.1117/1.JNP.14.026005.
38. Goyal, A. K., et al., "Performance analysis of Bloch surface wave-based sensor using transition metal dichalcogenides," *Applied Nanoscience*, 2020, doi: 10.1007/s13204-020-01538-0.
39. Quyang, Q., et al., "Sensitivity enhancement of transition metal dichalcogenides/silicon nanostructure-based surface plasmon resonance biosensor," *Sci. Rep.*, Vol. 6, 28190, 2016.
40. Rebhi, S. and M. Najjar, "High Q-factor optical filter with high refractive index sensitivity based on hourglass-shaped photonic crystal ring resonator," *Optik*, Vol. 202, 163663, 2020.
41. Farmani, H., et al., "A label-free graphene-based nanosensor using surface plasmon resonance for biomaterials detection," *Physica E: Low-dimensional Systems and Nanostructures*, Vol. 116, 113730, 2020.